Photochemistry and Photobiology, 2007, 83: 584–591

Study of Singlet Oxygen Equilibrium in Dioctadecyldimethylammonium Chloride Vesicles Employing 2-(n-(*N,N,N*-trimethylamine)-n-alkyl)-5-alkylfuryl Halides†

Antonio L. Zanocco*, Mónica Meléndrez, Germán Günther and Else Lemp

Universidad de Chile, Facultad de Ciencias Químicas y Farmacéuticas, Departamento de Química Orgánica y Fisicoquímica, Santiago, Chile

Received 1 August 2006; accepted 15 November 2006; published online 20 November 2006; DOI: 10.1562/2006-08-01-RA-991

ABSTRACT

Steady state photolysis and time resolved near infrared luminescence detection were employed to study the reaction kinetics of singlet oxygen with three different lipid-soluble probes incorporated in large unilamellar dioctadecyldimethylammonium chloride (DODAC) vesicles. The probes: 2-(4-(*N,N,N*-trimethylamine)-butyl)-5-dodecylfuryl bromide (DFTA), 2-(12-(*N,N,N*-trimethylamine)-dodecyl)-5-hexylfuryl bromide (HFDA) and 2-(1-(*N,N,N*-trimethylamine)-methyl)-5-methylfuryl iodide (MFMA) are useful in studying both singlet oxygen dynamics and its equilibrium in microcompartmentalized systems because they are actinometers in lipidic microphases. These probes contain a reactive furan ring, which will be located at different depths in the bilayer of DODAC vesicles. In the limit of the approximations, the result indicates an inhomogeneous equilibrium distribution of singlet oxygen across the bilayer. The calculated mean partitioning constant of singlet oxygen equals 2.8 and 8.3 at 20°C and 40°C, respectively, in the order of the previously reported constants for other microorganized systems such as sodium dodecylsulfate and cetyltrimethylammonium halide micelles and water/oil microemulsions.

INTRODUCTION

Oxygen is the most prevalent element in the earth's crust and one of the most relevant molecules in the maintenance of life (1). In spite of the enormous significance of this molecule, current investigations on oxygen and oxygen-related processes constitute a continuing challenge, and studies involving the first excited state of the oxygen molecule are of particular interest. Singlet molecular oxygen, $O_2(^1\Delta_g)$, reactions are important in biological systems, where they play important deleterious and/or beneficial roles, *e.g.* in photoinduced damage of tissues and photodynamic therapy of cancer (2–4). Analysis of singlet oxygen-mediated chemical processes in biological systems requires evaluation of its reactivity towards different acceptors present in very complex organizations. A critical characteristic of biological systems is their microheterogeneity. Consequently, gradients can occur in both the local singlet oxygen concentration and its reactivity. Therefore, detection of singlet molecular oxygen in biological systems is a complex task. Recent progress in detecting and quantifying singlet oxygen in biological systems involves the use of specific fluorescent probes such as DanePy and singlet oxygen sensor green, combined with fluorescence microscopy (5,6). Recently, there has been a great effort to develop singlet oxygen emission and two photon singlet oxygen microscopes (7–9). These systems allow the creation of singlet oxygen optical images of several materials including phase-separated liquids, polymeric samples and single cells (10). In the near future, singlet oxygen microscopes will be powerful tools in analyzing the spatially dependent roles played by singlet oxygen in photoinduced events that result in the death of biological cells and could also be applied to the study of singlet oxygen endogenously generated by both plant and animal cells. However, these systems are currently available in a very few laboratories and the most frequently used method to study singlet molecular oxygen processes involves fast response detectors with near-IR sensitivity. These detectors allow direct detection of $O_2(^1\Delta_g)$ by analyzing its weak emission at 1270 nm in both laser-pulsed flash photolysis and steady state experiments (11–13). However, this technique in biological systems has various limitations (14–16). As alternative, chemical trapping with well-designed water-soluble and/or lipid-soluble singlet oxygen acceptors would be an easily accessible tool to increase understanding of singlet oxygen behavior in microheterogeneous systems. The measurement of $O_2(^1\Delta_g)$ concentration in the aqueous pseudophase of these systems with acceptors or quenchers is difficult because of the low water solubility of potentially useful molecules (17,18). Most successful compounds for this kind of experiment include water-soluble derivatives of anthracene and 1,3-diphenylisobenzofuran (DPBF) (19,20). Therefore, the influence of lipid bilayers on the reactivity of the singlet oxygen acceptors incorporated in them and the relationship between acceptor localization and the eventual protective effect of the microenvironment should be studied. The ability of singlet oxygen to permeate through lipid bilayers can be studied by employing a water-soluble acceptor able to quench with zero-order kinetics, all the $O_2(^1\Delta_g)$ entering or leaving the bilayer (20).

In a previous study (21), we reported on the syntheses of several lipid-soluble singlet oxygen quenchers, with a furan moiety in their structure and anchored to the water-lipid

†This paper is part of a symposium-in-print dedicated to Professor Eduardo A. Lissi on the occasion of his 70th birthday.

*Corresponding author email: azanocco@ciq.uchile.cl (Antonio L. Zanocco)

interphase by a charged head group. These compounds should be useful in studying singlet oxygen dynamics and estimating steady state singlet oxygen concentrations at different depths in the bilayer, if there are appropriate spacers between the charged head group and the reactive moiety. We show that these probes react very rapidly with singlet oxygen through the chemical path, physical quenching can be neglected and medium effects on reactivity are small. The dependence of the singlet oxygen lifetime, τ, on the quencher concentration follows a behavior typically observed in microheterogeneous systems, where τ decreases linearly at low concentrations of the furan derivative, indicating that singlet oxygen equilibrates between the microphases. At higher quencher concentrations, τ becomes approximately constant indicating bilayer saturation.

The transport of small molecules across lipid membranes is a biological process of great importance. Most biologically significant transport processes across membranes involve some regulatory mechanism. Small, uncharged molecules such as water, oxygen, formamide and urea, however, permeate the membrane *via* a basal pathway at an appreciable rate. Even in the presence of channels, the major route of water permeation through plasma membranes seems to be through the lipid bilayer (22). The observed permeation rates are often qualitatively explained by means of a homogeneous solubility-diffusion model (23–25), which originally was developed to describe permeation through polymer membranes. In this model, permeation is described as a three-stage process: first, the molecule dissolves in the membrane, then diffuses through the membrane interior, and finally has to dissolve in the surrounding phase. This mechanism explains permeation of small molecules across polymer membranes. As this model is simple and works so well (even quantitatively) for water permeation, it has been widely used to describe permeation of other molecules across the membrane. However, molecular dynamics simulations show that the homogeneous solubility-fusion mechanism is not adequate to describe the permeation of small, uncharged molecules through a lipid membrane. Treating the membrane as a well-defined two-phase system like alkane/water is an oversimplification. Theoretical studies suggest that a four-region model is needed to describe permeation through the membrane (26–28). It is a qualitative model, based on simulation of the lipid membrane in combination with relevant experimental and theoretical data that divides the membrane into four distinct regions and contains the necessary details to understand permeation qualitatively.

With the aim of determining if an inhomogeneous equilibrium distribution of singlet oxygen is established across the bilayer when singlet oxygen is generated in the aqueous pseudophase, we used steady state photolysis and time-resolved singlet oxygen near IR luminescence detection to study the reaction kinetics of singlet oxygen with three lipid-soluble singlet oxygen probes incorporated in large unilamellar vesicles (LUVs) of dioctadecyldimethylammonium chloride (DODAC). The singlet oxygen probes (Fig. 1) are 2,5-disubstituted furan derivatives with different length alkyl chains and a terminal trimethylammonium head group in one of them. These molecules are anchored to the water–DODAC vesicle interphase by the charged head, allowing localization of the furan moieties at different depths in the bilayer. All our experiments were carried out at low quencher concentrations, typically 1:100 probe to detergent. This assures that singlet oxygen is equilibrated between the vesicle and the aqueous pseudophase and the bilayer is almost unperturbed by the probe.

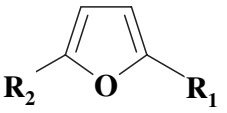

	R_1	R_2
DFTA	$C_{12}H_{25}$	$C_4H_6N^+(CH_3)_3Br^-$
HFDA	C_6H_{13}	$C_{12}H_{24}N^+(CH_3)_3Br^-$
MFMA	CH_3	$CH_2N^+(CH_3)_3I^-$

Figure 1. Structures of 2-(n-(*N*,*N*,*N*-trimethylamine)-n-alkyl)-5-alkyl-furyl halides.

MATERIALS AND METHODS

All solvents used in the syntheses and in spectroscopic and kinetic measurements were reagent grade, spectroscopic or HPLC quality. 2-(4-(*N*,*N*,*N*-trimethylamine)-butyl)-5-dodecylfuryl bromide (DFTA), 2-(12-(*N*,*N*,*N*-trimethylamine)-dodecyl)-5-hexylfuryl bromide (HFDA) and 2-(1-(*N*,*N*,*N*-trimethylamine)-methyl)-5-methylfuryl iodide (MFMA) were synthesized as previously described (21). Methylene blue (MB) and DPBF (Aldrich) was used as received. DODAC (Herga Ind.) was purified as described (29).

Time-resolved luminescence measurements were carried out in 0.5 cm path fluorescence cells at 20°C or 40°C. The MB sensitizer was excited with the 500 ps light pulse of a PTI model PL-202 dye laser (666 nm, *ca.* 200 μJ per pulse). A PTI model PL-2300 nitrogen laser was employed to pump the dye laser. A liquid-nitrogen cooled North Coast model EO-817P germanium photodiode detector with a built-in preamplifier was used to detect infrared radiation from the cell. The detector was at a right-angle to the cell. An interference filter (1270 nm; Spectrogon US, Inc.) and a cut-off filter (995 nm; Andover Corporation) were the only elements between the cell face and the diode cover plate. Preamplifier output was fed into the 1 MΩ input of a digitizing oscilloscope Hewlett Packard model 54540 A. Computerized experiment control, data acquisition and analysis were performed with LabView-based software developed in our laboratory.

Chemical reaction rate constants were determined in 10 m*M* DODAC vesicular solutions using a 10 mL double wall cell, light-protected by black paint. A centered window allowed irradiation with light of a given wavelength by using Schott cut-off filters. Circulating water maintained the cell temperature at 20 ± 0.5°C or 40 ± 0.5°C. The irradiation of the sensitizer was performed with a visible, 200 W, Par lamp. A Waters 600 liquid chromatograph equipped with a PDA detector Waters 996 and a Waters Delta Pack C-4 (3.9 × 150 mm) HPLC column was used to monitor furan derivative consumption.

LUVs of DODAC were obtained by controlled injection of a DODAC–chloroform solution (20 m*M*) into 5 mL D_2O (Aldrich) at 75 ± 0.5°C, as described (30). The final concentration was fixed by the amount of injected DODAC–chloroform solution. LUVs with furan derivatives incorporated in the lipidic bilayer were obtained by using the same procedure, but first adding an appropriate amount of probe to the DODAC–chloroform solution.

RESULTS AND DISCUSSION

Singlet oxygen luminescence quenching by furan derivatives

In homogeneous media, singlet oxygen reaction with a furan derivative, *F*, involves physical (deactivation) and/or chemical (reactive) processes, as represented in the simplified mechanism (Scheme 1): where k_d is the solvent-dependent decay rate constant of singlet oxygen that determines its intrinsic lifetime in the given solvent ($\tau_o = 1/k_d$), k_{Ph} is the second-order rate constant of the physical quenching and k_r is the second-order rate constant of the reactive pathway.

$$O_2 \xrightarrow{sens} {}^1O_2 \quad (1)$$

$${}^1O_2 \xrightarrow{k_d} O_2 \quad (2)$$

$${}^1O_2 + F \xrightarrow{k_{ph}} \text{Physical quenching} \quad (3)$$

$${}^1O_2 + F \xrightarrow{k_r} \text{Products} \quad (4)$$

Scheme 1

We had previously shown that the reaction of singlet oxygen with DFTA, HFDA and MFMA in homogeneous solvents occurs mainly through the chemical path ($k_T = k_{ph} + k_r \approx k_r$), and that k_T values are almost solvent independent (21). Representative total rate constants for several furan derivatives—including 2-methylfuran and 2,5-dimethylfuran—are shown in Table 1. With DPBF as actinometer, k_r(DPBF) = 1.0×10^9 M^{-1} s^{-1} (31), we determined k_r(DFTA) and k_r(HFDA) in ethanol as $(3.1 \pm 0.30) \times 10^8$ M^{-1} s^{-1} and $(2.9 \pm 0.26) \times 10^8$ M^{-1} s^{-1}, respectively. These values are very close to those measured by time-resolved methods for these compounds in the same solvent (Table 1). This result indicates that the reaction of singlet oxygen with DFTA and HFDA occurs mainly through the chemical path and in homogeneous solvent; $k_T = k_{ph} + k_r \approx k_r$. The behavior is similar to that observed for 2,5-dimethylfuran (2,5-DMF) (32,33). These are not novel results because it has been reported that furan derivatives quench singlet oxygen only through the chemical pathway to yield endoperoxides (34–36), but it is important to demonstrate that for the singlet oxygen probes employed in this work, the physical contribution to singlet oxygen quenching is negligible.

Data in Table 1 show considerable differences in the reactivities of furan derivatives towards singlet oxygen. Monosubstituted derivatives such as 2-methylfuran show that k_T increases by about 12-fold when solvent changes from nonpolar to nonprotic polar. On the contrary, reactivities of 2,5-disubstituted furans are nearly media independent. For example k_T values for 2,5-DMF measured in a large set of solvents increases only by a factor of four when the solvent is changed from hexane to propylencarbonate. Most noteworthy is the fact that for this compound values of k_T are very similar in solvents with similar microscopic properties such as nonpolar hydrocarbons or polar protic alcohols. An extensive study of the reactivity dependence on the media for the furan derivatives used as singlet oxygen scavengers in vesicular solutions has not been made, as amphiphatic structures limit the solvent set in which they can be studied. However, the kinetic data included in Table 1 indicate that a very similar behavior to that observed for 2,5-DMF must be expected for these compounds.

Scheme 2 shows a physical model with the minimum requirements to explain singlet oxygen decay and reactions in microheterogeneous systems such as micelles, reverse micelles,

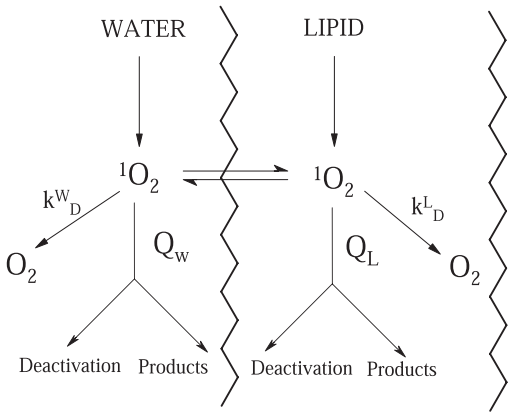

Scheme 2

Table 1. Values of the total rate constants, k_T, for reaction of singlet oxygen with furan derivatives in different media at 20°C.

	$k_T/10^8$ M^{-1} s^{-1}				
Solvent	2-Methylfuran*	2,5-DMF†	DFTA	HFDA	MFMA
n-Hexane	0.25 ± 0.13	2.11 ± 0.08	1.81 ± 0.10 2.11 ± 0.15‡	1.90 ± 0.12 2.23 ± 0.13‡	2.78 ± 0.18
n-Heptane	–	2.39 ± 0.10	1.92 ± 0.21	1.88 ± 0.17	–
n-Octanol	0.72 ± 0.29	–	–	–	–
n-Hexanol	0,75 ± 0,30	–	–	–	–
Benzene	1.22 ± 0.62	5.06 ± 0.20	2.81 ± 0.11	3.48 ± 0.14	2.60 ± 0.14
Ethyl acetate	0.98 ± 0.51	4.44 ± 0.18	–	–	
Acetonitrile	1.88 ± 1.01	3.39 ± 0.10	4.43 ± 0.38	4.23 ± 0.16	2.06 ± 0.12
Chloroform	–	2.96 ± 0.08	1.86 ± 0.06		–
Acetone	1.39 ± 0.71	4.45 ± 0.18	–	–	–
Methylene dichloride	1.11 ± 0.58	4.02 ± 0.12	–	–	–
Methanol	1.16 ± 0.62	5.33 ± 0.27	–	–	–
Ethanol	0.83 ± 0.54	3.33 ± 0.13	3.08 ± 0.27 (3.10 ± 0.30)	3.12 ± 0.09 (2.96 ± 0.26)	
n-Propanol	0.88 ± 0.69	4.18 ± 0.17	–	–	–
Benzyl alcohol	2.41 ± 1.45	7.46 ± 0.30	3.50 ± 0.14	–	–
Dimethylformamide	2.84 ± 1.53	7.94 ± 0.31	–	–	–
Benzonitrile	2.02 ± 1.04	6.50 ± 0.26	–	–	–
Propylencarbonate	2.90 ± 1.62	8.58 ± 0.34	–	–	–
D_2O	–	4.43 ± 0.18	3.41 ± 0.29	2.69 ± 0.13	1.37 ± 0.12 1.50 ± 0.09‡

*From reference (37). †From reference (16). ‡Values at 40°C. HFDA, 2-(12-(*N*,*N*,*N*-trimethylamine)-dodecyl)-5-hexylfuryl bromide; DFTA, 2-(4-(*N*,*N*,*N*-trimethylamine)-butyl)-5-dodecylfuryl bromide; MFMA, 2-(1-(*N*,*N*,*N*-trimethylamine)-methyl)-5-methylfuryl iodide.

vesicles and simple single membrane biological systems (such as red blood cell ghosts or microsomes) (16).

This model includes the external aqueous solvent and the vesicle membrane bilayer as pseudophases. In our experiments, singlet oxygen was generated in the aqueous external pseudophase employing MB (ϕ_Δ = 0.5 in water) (38) as the sensitizer. MB was added to DODAC vesicular solutions just before performing measurements. For DODAC vesicles, MB permeation through the bilayer is negligible at room temperature (20 ± 2°C) (39). In addition, we consider that DFTA and HFDA should be located exclusively in the lipidic pseudophase, because of the structural similarity with anthracene and pyrene derivatives currently employed as fluorescent probes in vesicles of synthetic and natural surfactants (40–44). The trimethylammonium head and the length of the tether alkyl group locate the reactive furan moiety at different depths in the vesicle bilayer. On the assumption that alkyl groups are extended, we can say that when DFTA is the probe, the furan group is located in an intermediate region of the bilayer; and when HFDA is the probe, the reactive group is deeper inside the bilayer. On the other hand, when MFMA is the probe, we assume that the reactive group is located near the water-lipid bilayer interphase (in ultrafiltration experiments of DODAC vesicles loaded with MFMA it was not detected in the continuous solvent).

According to the simplest model (45), the value of the rate constant for the near IR luminescence decay of singlet oxygen, k_D, measured in DODAC vesicles with furan derivatives anchored to the bilayer, is given by:

$$k_D = k_d + (1 - f)k_{T,L}[F]_L \quad (5)$$

where f is the fraction of singlet oxygen in the aqueous pseudophase, $k_{T,L}$ is the total quenching rate constant in the bilayer and $[F]_L$ is the local quencher concentration expressed in moles L^{-1} of microaggregate. The singlet oxygen partitioning constant, K, between the bilayer and the aqueous pseudophase is defined as:

$$K = [O_2(^1\Delta_g)]_L/[O_2(^1\Delta_g)]_W \quad (6)$$

where $[O_2(^1\Delta_g)]_L$ and $[O_2(^1\Delta_g)]_W$ are singlet oxygen concentrations in the bilayer and the external solvent, respectively. Equation (6) can be expressed in terms of n_L and n_W, the singlet oxygen moles in the lipidic and the aqueous pseudophase, respectively:

$$K = n_L V_W/n_W V_L \quad (7)$$

where V_L and V_W are the volume of the lipidic and the aqueous pseudophase, respectively. Dividing by n_T, the total singlet oxygen moles present in the vesicular solution, the singlet oxygen partitioning constant can be expressed in terms of the fraction of singlet oxygen in the aqueous pseudophase, f:

$$K = (V_W/V_L)[(1 - f)/f] \quad (8)$$

considering that $f \to 1$ in vesicular solutions (16), expressing the local quencher concentration in terms of the analytical quencher concentration, $[F]_L = (V_W/V_L)[F]$ and replacing it in Eq. (5):

$$k_D = k_d + Kk_{T,L}[F] \quad (9)$$

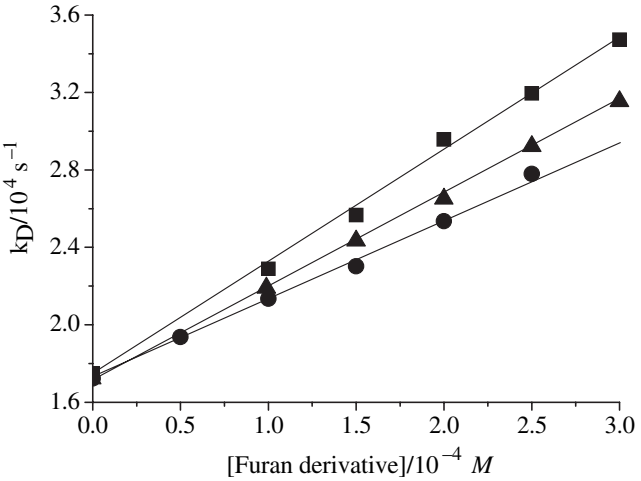

Figure 2. Stern–Volmer type plot for singlet oxygen deactivation by furan derivatives in 10 mM DODAC vesicles with MB as sensitizer at 20°C. MFMA ■, DFTA ▲ and HFDA ●.

where $[F]$ is the analytical quencher concentration. Equation (9) shows that the slope of a Stern–Volmer plot in a system described in terms of the two-pseudophase model corresponds to an apparent second-order rate constant:

$$k_{app} = Kk_{T,L} \quad (10)$$

Figure 2 shows the Stern–Volmer plots obtained from the singlet oxygen luminescence decay quenching with each furan derivative anchored to the lipidic bilayer. In all cases, there is a linear dependence of k_d on quencher concentrations. The values of k_{app} obtained from the slopes of these plots (the mean value of at least five independent experiments) are included in Table 2. At the limit of zero furan concentration (*i.e.* the intercept), the data indicate a lifetime of approximately 55–60 μs. This lifetime is close to that measured in pure D_2O indicating that singlet oxygen is rapidly equilibrated between the outside and inside of the membrane. Independent experiments (data not reported) show that up to 15 mM of DODAC diminishes the singlet oxygen lifetime in D_2O by less than 5%.

Furthermore, according to Eq. (10) differences in the k_{app} values could be caused by distinct reactivities of the singlet

Table 2. Values of k_{app} for reaction of singlet oxygen with furan derivatives in 10 mM DODAC vesicles with MB (1.39×10^{-5} M) as sensitizer.

	$k_{app}/10^8\ M^{-1}\ s^{-1}$	
	20°C	40°C
HFDA	0.41 ± 0.06	2.10 ± 0.12
DFTA	0.48 ± 0.08	2.00 ± 0.11
MFMA	0.58 ± 0.08	1.30 ± 0.09

DODAC, dioctadecyldimethylammonium chloride; MB, methylene blue; HFDA, 2-(12-(*N*,*N*,*N*-trimethylamine)-dodecyl)-5-hexylfuryl bromide; DFTA, 2-(4-(*N*,*N*,*N*-trimethylamine)-butyl)-5-dodecylfuryl bromide; MFMA, 2-(1-(*N*,*N*,*N*-trimethylamine)-methyl)-5-methylfuryl iodide.

oxygen probes incorporated in the bilayer and/or by differences in the singlet oxygen concentration sensed by each probe in the furan moiety site. This latter effect may be caused by an inhomogeneous singlet oxygen partitioning across the bilayer due to morphological differences in the microenvironment sensed by each probe.

HPLC analysis of consumption of the furan derivative

We determined the values for k_{exp}, the pseudo first-order rate constant for the chemical reactions of DFTA, HFDA and MFMA with singlet oxygen in 10 m*M* DODAC vesicular solutions by following the consumption of furan derivatives by HPLC. A typical plot showing that consumption MFMA at 20°C fits first-order kinetics can be seen in Fig. 3. Similar behaviors were observed for MFMA at 40°C and for DFTA and HFDA at 20°C and 40°C.

Values of k_{exp} at 20°C and 40°C for the singlet oxygen reaction with the furan derivatives by using MB as sensitizer are included in Table 3, as the mean of at least five independent experiments.

The data in Table 3 obtained at constant MB concentration show k_{exp} values following the order $k_{exp}^{DFTA} > k_{exp}^{MFMA} > k_{exp}^{HFDA}$ at 20°C and $k_{exp}^{HFDA} > k_{exp}^{DFTA} > k_{exp}^{MFMA}$ at 40°C. According to the two-pseudophase model, the slope of the first-order plots, k_{exp}, obtained in steady state experiments by following the furan consumption in vesicular solutions with furan anchored to the bilayer is:

$$k_{exp} = k_{r,L}[O_2(^1\Delta_g)]_{L,F} \quad (11)$$

where $k_{r,L}$ is the singlet oxygen chemical reaction rate constant in the bilayer and $[O_2(^1\Delta_g)]_{L,F}$ is the singlet oxygen concentration in the probe microenvironment within the bilayer.

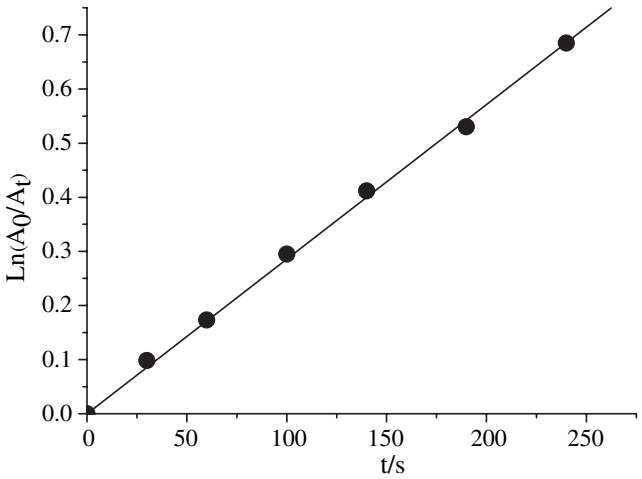

Figure 3. First-order plot for DFTA consumption in 10 m*M* DODAC vesicles with MB (1.39×10^{-5} *M*) as sensitizer at 20°C.

Table 3. Values of k_{exp} at 20°C and 40°C for singlet oxygen reaction with furan derivatives in 10 m*M* DODAC vesicles with MB (1.39×10^{-5} *M*) as sensitizer.

	$k_{exp}/10^{-3}$ s^{-1}	
	20°C	40°C
HFDA	2.35 ± 0.15	8.00 ± 0.61
DFTA	4.78 ± 0.29	6.34 ± 0.56
MFMA	2.81 ± 0.18	3.41 ± 0.41

DODAC, dioctadecyldimethylammonium chloride; MB, methylene blue; HFDA, 2-(12-(*N*,*N*,*N*-trimethylamine)-dodecyl)-5-hexylfuryl bromide; DFTA, 2-(4-(*N*,*N*,*N*-trimethylamine)-butyl)-5-dodecylfuryl bromide; MFMA, 2-(1-(*N*,*N*,*N*-trimethylamine)-methyl)-5-methylfuryl iodide.

Model for the distribution of singlet oxygen across the bilayer

The homogeneous solubility-diffusion model has currently been invoked to explain the physicochemical behavior of small molecules in lipid bilayers. When it is applied to lipid membranes, they have been regarded as a homogeneous phase resembling liquid alkanes with well-defined boundaries, separated from the water phase. According to the basis of this model, a homogeneous distribution of singlet oxygen throughout the lipidic pseudophase is predicted and this microenvironment should be sensed by the three probes employed. Considering the k_{exp} and k_{app} values obtained with the different probes in vesicular solutions, the homogeneous solubility-diffusion model seems to be inadequate.

Our results can be ascribed to different singlet oxygen concentrations sensed by the probes. Also the probes could react at different rates with singlet oxygen due to the furan ring being located at different depths for each probe, and sensing different microenvironments in the bilayer. Therefore, both a "local" singlet oxygen concentration and a "local" singlet oxygen partitioning constant can be defined and calculated from time-resolved and steady-state kinetics observed for each furan derivative.

In order to obtain a nearly quantitative approach to singlet oxygen distribution in the DODAC vesicles bilayer, we applied the bilayer model of Marrink (26–28), which has been employed to account for diffusion rate profiles, resistance to permeation, the accessible free volume distribution and the excess free energy profiles for the small molecules in dipalmitoylphosphatidylcholine (DPPC) liposomes. In the model, the lipidic bilayer can be described in terms of the existence of four regions. Region 1 includes low density head groups with loosely bound water, region 2 comprises the high density head groups and strongly bound water, region 3 contains the more ordered part of lipid tails with high density akin to liquid hexadecane and region 4 involves the major part of the lipid end groups, this region is more disordered with a density such as fluid decane. Applying this model to DODAC vesicles, the reactive moieties of the singlet oxygen probes MFMA, HFDA and DFTA would be located in regions 2, 3 and 4, respectively, as schematically represented in Fig. 4. If the probes are fully extended as shown in Fig. 4, the microenvironment sensed by DFTA and HFDA should be similar to hexadecane and decane, respectively. In addition, MFMA, located at the interphase, should sense a highly polar protic microenvironment rich in free and bounded water molecules (46,47).

The 2,5-dialkylfurans such as 2,5-dimethylfuran, DFTA, and HFMA have similar quenching rate constants with a small solvent dependence, whereas MFMA behaves slightly differently (21). In hydrocarbon solvents such as decane and

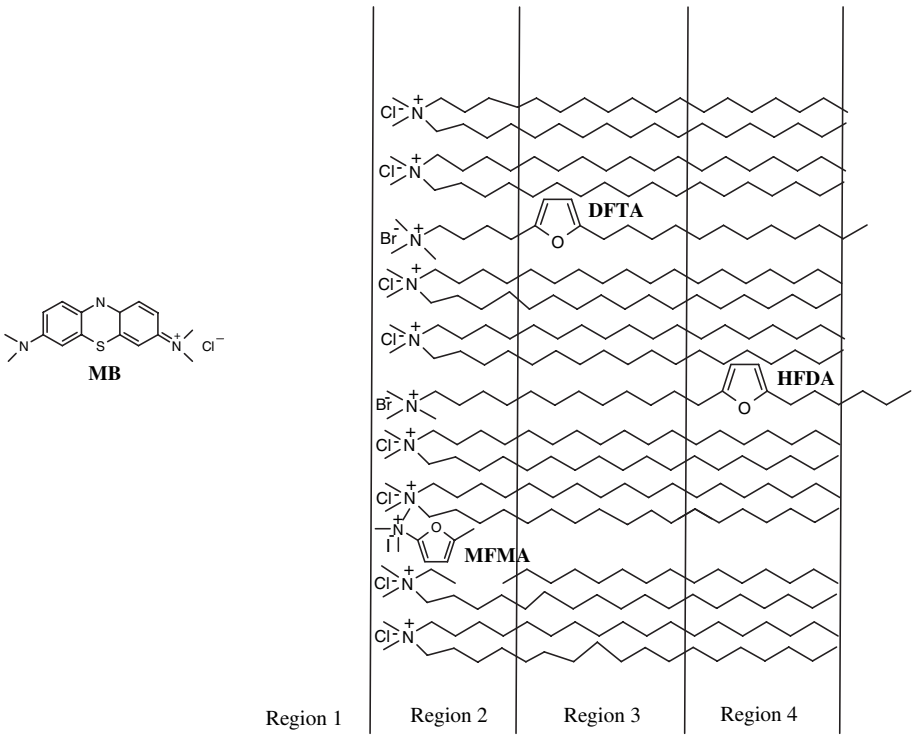

Figure 4. Schematic representation of DODAC liposome bilayer according to the model of Marrink (26,27). The relative locations of the singlet oxygen probes MFMA, DFTA and HFDA and the sensitizer MB are illustrated.

hexadecane, measurements of both k_T and k_r for DFTA and HFDA were not possible because of their low solubility. We determined k_T values for reactions of singlet oxygen with DFTA and HFDA in hexane and heptane (Table 1). In addition, our studies of the solvent effect on the reactivity of 2,5-dimethylfuran towards singlet oxygen (48) indicate that the total rate constant does not increase by more than 10% when the solvent is changed from hexane to decane. Then, considering that for DFTA and HFDA, k_T values are almost solvent independent and the reactive furan group of these molecules should be located in highly nonpolar regions of the bilayer, we propose that, for DFTA and HFDA, $k_{T,L} \approx k_{r,L} \approx k_T$(hexane) and for MFMA, near the interphase, $k_{T,L} \approx k_{r,L} \approx k_T$(water) as a reasonable approximation. In these expressions, the subscript L stands for the reaction rate constants expressed in terms of lipidic pseudophase volume. Thus Eqs. (10) and (11) can be rewritten as:

$$K = k_{app}/k_{T,L} = k_{app}k_T(\text{solvent}) \quad (12)$$

$$[O_2(^1\Delta_g)]_{L,F} = k_{exp}/k_{r,L} = k_{exp}/k_T(\text{solvent}) \quad (13)$$

The k_T(solvent) values for HFDA, DFTA and MFMA at 20°C and 40°C are included in Table 1. To express k_T(solvent) in terms of the lipidic pseudophase volume, the ratio between the vesicular volume and the aqueous pseudophase volume was calculated by using structural parameters for large DODAC vesicles reported by Carmona-Ribeiro *et al.*: *e.g.* bilayer thickness of 5 nm, head group cross section of 0.43 Å and an aggregation number of 3.58×10^6 surfactant molecules/vesicle (49,50).

Equations (12) and (13) show that both the "local" singlet oxygen partitioning constant and the "local" singlet oxygen steady-state concentration sensed by the different probes can be experimentally evaluated. The values obtained are shown in Table 4.

If the values for "local" singlet oxygen steady-state concentrations at 40°C, above the gel-to-liquid crystalline transition phase of DODAC vesicles are considered, we note an increase of 50% when moving from region 2 to region 4 of the bilayer. A similar trend is shown by the "local" partitioning constant. So far as we know, no reports have been published on experimentally observed inhomogeneity in the

Table 4. Values of the "local" singlet oxygen partitioning constant and the "local" singlet oxygen steady-state concentration at 20°C and 40°C in 10 m*M* DODAC vesicular solutions with MB (1.39×10^{-5} *M*) as the sensitizer.

	$[O_2(^1\Delta_g)]_{L,F}$/ 10^{-10} *M*		*K*		k_T(solvent)/10^8 M^{-1} s^{-1}	
	20°C	40°C	20°C	40°C	20°C	40°C
HFDA	1.1 ± 0.14	3.3 ± 0.42	2.0 ± 0.4	8.6 ± 1.2	1.90 ± 0.12	2.23 ± 0.13
DFTA	2.6 ± 0.27	2.7 ± 0.43	2.4 ± 0.5	8.5 ± 1.1	1.81 ± 0.10	2.11 ± 0.15
MFMA	1.9 ± 0.28	2.1 ± 0.36	3.8 ± 0.8	7.9 ± 1.3	1.37 ± 0.12	1.50 ± 0.09

DODAC, dioctadecyldimethylammonium chloride; MB, methylene blue; HFDA, 2-(12-(*N*,*N*,*N*-trimethylamine)-dodecyl)-5-hexylfuryl bromide; DFTA, 2-(4-(*N*,*N*,*N*-trimethylamine)-butyl)-5-dodecylfuryl bromide; MFMA, 2-(1-(*N*,*N*,*N*-trimethylamine)-methyl)-5-methylfuryl iodide.

concentration of a small molecule across a simple lipidic bilayer. However, theoretical calculations for the excess free energy profiles of oxygen molecule in a DPPC vesicle bilayer above the transition phase temperature (27) predict that for the hydrophobic oxygen molecule the solubility increases when the molecule goes from the region 1 to the region 4 (see Fig. 4). This theoretical picture of small, neutral and hydrophobic molecule permeation supported by an inhomogeneous solubility-diffusion model, allows to explain the observed changes in "local" singlet oxygen steady state concentrations sensed by the probes located at different depths in a DODAC vesicle bilayer, in spite of the uncertainty of our values and the approximations employed in our calculations. In particular, a different choice of solvents to mimic each region would lead to different values of the "local" properties, but those employed (k_T in hexane to mimic regions 3 and 4 and k_T in water to mimic region 2) correspond to the more suitable values available, if experimental and theoretical studies regarding the bilayer composition and structure are considered. Data obtained at 20°C are hard to understand and neither experimental nor theoretical reports have been published on a detailed structure of simple vesicle bilayer in the gel state. The results would be compatible with an inhomogeneous distribution of singlet oxygen concentration across the DODAC vesicle bilayer at this temperature. The region sensed by DFTA (region 3) is one with the highest capacity to solubilize singlet oxygen.

In order to compare the present data with those reported in literature for other microheterogeneous systems, we found appropriate to define a total mean value of the singlet oxygen steady state concentration in terms of the volume fraction for each region. To calculate the volume fraction for each region, we assume proportionality between the radial thickness of the regions 2, 3 and 4 of the Marrink model (26,28) when DPPC and DODAC vesicles are compared (hexadecyl tails *vs* octadecyl tails). In addition, we neglect the contribution of region 1, which essentially belongs to the aqueous pseudophase, to the singlet oxygen equilibrium. Then, employing the structural parameters for large DODAC vesicles (49,50), we found volume fractions of 0.38, 0.35 and 0.27, for region 2 (radial thickness ≈0.94 nm), 3 (radial thickness ≈0.89 nm) and 4 (radial thickness ≈0.67 nm), respectively. According to these approximations, the mean steady state singlet oxygen concentration can be calculated by Eq. (14):

$$[^1O_2]_{MEAN} = 0.38[^1O_2]_{MFMA} + 0.35[^1O_2]_{DFTA} + 0.27[^1O_2]_{HFDA} \quad (14)$$

where $[^1O_2]_{MFMA}$, $[^1O_2]_{DFTA}$ and $[^1O_2]_{HFDA}$ correspond to the "local" singlet oxygen concentrations sensed by the different probes. The mean singlet oxygen concentrations calculated from Eq. (14) were equal to 1.9×10^{-10} *M* and 2.6×10^{-10} *M* at 20°C and 40°C, respectively. If an analogous equation is defined in order to calculate a mean equilibrium constant, we find values of 2.8 and 8.3 at 20°C and 40°C, respectively. Although no data have been published regarding singlet oxygen equilibrium in vesicular solutions, the values determined in this study compare favorably with those reported by Rodgers *et al.* (45) (*K* values equal to 2.9 and 4.1 for SDS and CTAB micelles, respectively) and Oliveros *et al.* (51) (*K* values equal to 4.1 and 5.3 for SDS and CTAC micelles, respectively). In several water/oil (W/O) microemulsions of different composition and with different surfactants, values of *K* are equal to 4.2, 6.1 and 9.0 (45,51,52).

In conclusion, 2-(n-(*N*,*N*,*N*-trimethyl)-n-alkyl)-5-alkylfuryl halides are useful probes for studying singlet oxygen dynamics and equilibria in microcompartmentalized systems because they fulfill all the conditions as actinometers in lipidic microphases. The data obtained with these probes with the reactive moiety located at different depths in the bilayer of DODAC vesicles could indicate that an inhomogeneous distribution of singlet oxygen is established across the bilayer when singlet oxygen is generated by means of a sensitizer in the aqueous pseudophase. Furthermore, to our knowledge, equilibrium constants for singlet oxygen partitioning between the lipidic bilayer and the aqueous external pseudophase in DODAC vesicular solutions have been determined, for the first time, by employing steady-state and time-resolved kinetic measurements. The partitioning constants are in the order of those previously reported for other micro-organized systems such as SDS and CTAB micelles and W/O microemulsions, in spite of the approximations employed to calculate these values. Further experiments regarding singlet oxygen dynamics and equilibrium in other microheterogeneous systems such as micelles and DPPC vesicles are in progress in our laboratory.

Acknowledgement—The financial support from FONDECYT (grant 1030742) is gratefully acknowledged.

REFERENCES

1. Halliwell, B. and J. M. C. Gutteride (1999) *Free Radicals in Biology and Medicine*, pp. 1–33. Oxford University Press Inc., New York, NY.
2. Briviba, K., L.-O. Klotz and H. Sies (1997) Toxic and signaling effects of photochemically or chemically generated singlet oxygen in biological systems. *Biol. Chem.* **378**, 1259–1265.
3. Hultén, L. M., M. Holmström and B. Soussi (1999) Harmful singlet oxygen can be helpful. *Free Radic. Biol. Med.* **27**, 1203–1207.
4. Tarr, M. and D. P. Valenzeno (2003) Singlet oxygen: The relevance of extracellular production mechanisms to oxidative stress *in vivo*. *Photochem. Photobiol. Sci.* **2**, 355–361.
5. Tanaka, K., T. Miura, N. Umezawa, Y. Urano, K. Kikuchi, T. Higuchi and T. Nagano (2001) Rational design of fluorescein-based fluorescence probes. Mechanism-based design of a maximum fluorescence probe for singlet oxygen. *J. Am. Chem. Soc.* **123**, 2530–2536.
6. Hideg, È., T. Kálai, K. Hideg and I. Vass (1998) Photoinhibition of photosynthesis *in vivo* results in singlet oxygen production detection *via* nitroxide-induced fluorescence quenching in broad bean leaves. *Biochemistry* **37**, 11405–11411.
7. Snyder, J. W., I. Zebger, Z. Gao, L. Poulsen, P. K. Frederiksen, E. Skovsen, S. P. Mcilroy, M. Klinger, L. K. Andersen and P. R. Ogilby (2004) Singlet oxygen microscope: From phase-separated polymers to single biological cells. *Acc. Chem. Res.* **37**, 894–901.
8. Zebger, I., L. Poulsen, Z. Gao, L. K. Andersen and P. R. Ogilby (2003) Singlet oxygen images of heterogeneous samples: Examining the effect of singlet oxygen diffusion across the interfacial boundary in phase-separated liquids and polymers. *Langmuir* **19**, 8927–8933.
9. Andersen, L. K., Z. Gao, P. R. Ogilby, L. Poulsen and I. Zebger (2002) A singlet oxygen image with 2.5 μm resolution. *J. Phys. Chem. A* **106**, 8488–8490.
10. Skovsen, E., J. W. Snyder, J. D. C. Lambert and P. R. Ogilby (2005) Lifetime and diffusion of singlet oxygen in a cell. *J. Phys. Chem. B* **109**, 8570–8573.

11. Schweitzer, C. and R. Schmidt (2003) Physical mechanisms of generation and deactivation of singlet oxygen. *Chem. Rev.* **103**, 1685–1757.
12. Nonell, S. and S. E. Braslavsky (2000) Time-resolved singlet oxygen detection. *Methods Enzymol.* **319**, 37–49.
13. Oliveros, E., P. Murasecco-Suardi and A. M. Braun (1992) Efficiency of singlet oxygen quenching by carotenoids measured by near-infrared steady-state luminescence. *Methods Enzymol.* **213**, 420–429.
14. Rodgers, M. A. J. (1983) Solvent-induced deactivation of singlet oxygen: Additivity relationships in nonaromatic solvents. *J. Am. Chem. Soc.* **105**, 6201–6205.
15. Kiryua, Ch., M. Makiuchi, J. Miyazaki, T. Fujinaga and K. Kakinuma (1999) Physiological production of singlet molecular oxygen in the myeloperoxidase-H_2O_2-chloride system. *FEBS Lett.* **443**, 154–158.
16. Lissi, E. A., E. Lemp and A. L. Zanocco (2001) Singlet-oxygen reactions: Solvent and compartmentalization effects. In *Understanding and Manipulating Excited-States Processes* (Edited by V. Ramamurthy and K. S. Schanze), pp. 287–316. Marcel Dekker, New York.
17. Duran, N. (1982) Singlet oxygen in biological processes. In *Chemical and Biological Generation of Excited States* (Edited by W. Adam and G. Cilento), pp. 345–369. Academic Press, New York.
18. Foote, C. S. (1979) Quenching of singlet oxygen. In *Singlet Oxygen* (Edited by H. H. Wasserman and R.W. Murray), pp. 129–171. Academic Press, New York.
19. Lindig, B. A., M. A. J. Rodgers and A. P. Schaap (1980) Determination of the lifetime of singlet oxygen in D_2O using 9,l0-anthracenedipropionic acid, a water-soluble probe. *J. Am. Chem. Soc.* **102**, 5590–5593.
20. Amat-Guerri, F., E. Lemp, E. A. Lissi, F. J. Rodriguez and F. R. Trull (1996) Water-soluble 1,3-diphenylisobenzofuran derivatives. Synthesis and evaluation as singlet molecular oxygen acceptors for biological systems. *J. Photochem. Photobiol. A Chem.* **93**, 49–56.
21. Castañeda, F., A. L. Zanocco, M. Meléndrez, G. Günther and E. Lemp (2004) Synthesis of 2-(n-(N,N,N-trimethyl)-n-alkyl)-5-alkylfuryl halides. Useful probes for studying singlet oxygen dynamics and equilibria in microcompartmentalized systems. *J. Photochem. Photobiol. A Chem.* **168**, 175–183.
22. Finkelstein, A. (1984) *Current Topics in Membranes and Transport*, pp. 295–308. Academic Press, New York.
23. Hanai, T. and D. A. Daydon (1966) The permeability to water of bimolecular lipid membranes. *J. Theor. Biol.* **11**, 370–382.
24. Finkelstein, A. and A. Cass (1968) Effect of cholesterol on the water permeability of thin lipid membranes. *Nature* **216**, 717–718.
25. Träuble, H. (1971) The movement of molecules across lipid membranes: A molecular theory. *J. Membr. Biol.* **4**, 193–208.
26. Marrink, S. J. and H. J. C. Berendsen (1994) Simulation of water transport through a lipid-membrane. *J. Phys. Chem.* **98**, 4155–4168.
27. Marrink, S. J. and H. J. C. Berendsen (1996) Permeation process of small molecules across lipid membranes studied by molecular dynamics simulations. *J. Phys. Chem.* **100**, 16729–16738.
28. Marrink, S. J., R. M. Sok and H. J. C. Berendsen (1996) Free volume properties of a simulated lipid membrane. *J. Chem. Phys.* **104**, 9090–9099.
29. Barra, M., C. Bohne, A. L. Zanocco and J. C. Scaiano (1992) Exploratory-study of the application of transmission and diffuse-reflectance laser techniques in the study of free-radical processes in vesicles. *Langmuir* **8**, 2390–2395.
30. Encinas, M. V., E. Lemp and E. A. Lissi (1989) Vesicular effect on the reactivity of anthracene derivatives towards singlet molecular oxygen. *J. Photochem. Photobiol. B Biol.* **3**, 113–122.
31. Nowakowska, M. (1984) Solvent effect on the quantum yield of the self-sensitized photoperoxidation of 1,3-diphenylisobenzofuran. *J. Chem. Soc. Faraday Trans.* **1**(80), 2119–2126.
32. Gollnick, K. and K. Knutzen-Mies (1991) Dye-sensitized photooxygenation of 2,3-dihydrofurans: Competing [2 + 2] cycloadditions and ene reactions of singlet oxygen with a rigid cyclic enol ether system. *J. Org. Chem.* **56**, 4017–4027.
33. Usui, Y., M. Tsukada and H. Nakamura (1978) Kinetic studies of photosensitized oxygenation by singlet oxygen in aqueous micellar solutions. *Bull. Chem. Soc. Jpn.* **51**, 379–384.
34. Zanocco, A. L., G. Günther, E. Lemp, J. R. de la Fuente and N. Pizarro (1998) Kinetics and mechanism of the photosensitized oxidation of furosemide. *Photochem. Photobiol.* **68**, 487–493.
35. Clennan, E. L. (1991) Synthetic and mechanistic aspects of 1,3-diene photooxidation. *Tetrahedron* **47**, 1343–1382.
36. Gollnick, K. and A. Griesbeck (1985) Singlet oxygen photooxygenation of furans. Isolation and reactions of (4 + 2)-cycloaddition products (unsaturated sec.-ozonides). *Tetrahedron* **41**, 2057–2068.
37. Clennan, E. L. and M. E. Mehrsheikh-Mohammadi (1983) Addition of singlet oxygen to conjugated dienes. The mechanism of endoperoxide formation. *J. Am. Chem. Soc.* **105**, 5932–5933.
38. Usui, Y. and K. Kamogawa (1974) A standard system to determine the quantum yield of singlet oxygen formation in aqueous solution. *Photochem. Photobiol.* **19**, 245–247.
39. Zanocco, A. L., G. Günther, E. Lemp and E. A. Lissi (1998) Release of methylene blue from dioctadecyldimethylammonium chloride vesicles. *J. Chem. Soc. Perkin Trans.* **2**, 319–323.
40. Cooper, P. and J. B. Meddings (1991) Erythrocyte membrane fluidity in malignant hyperthermia. *Biochim. Biophys. Acta* **1069**, 151–156.
41. Villalain, J. and M. Prieto (1991) Location and interaction of *N*-(9-anthroyloxy)-stearic acid probes incorporated in phosphatidylcholine vesicles. *Chem. Phys. Lipids* **59**, 9–16.
42. L'Heureux, G. P. and M. Fragata (1987) Micropolarities of lipid bilayers and micelles: 4. Dielectric constant determinations of unilamellar phosphatidylcholine vesicles with the probes pyrene and 16-(1-pyrenyl)hexadecanoic acid. *J. Colloid. Interface Sci.* **117**, 513–522.
43. L'Heureux, G. P. and M. Fragata (1989) Monomeric and aggregated pyrene and 16-(1-pyrenyl)hexadecanoic acid in small, unilamellar phosphatidylcholine vesicles and ethanol—buffer solutions. *J. Photochem. Photobiol. B. Biol.* **3**, 53–63.
44. Soto, M. A., C. P. Sotomayor and E. A. Lissi (2002) Effect of gramicidin addition upon the physicochemical properties of dipalmitoyl phosphatidyl choline large unilamellar vesicles. *J. Photochem. Photobiol. A Chem.* **152**, 79–93.
45. Lee, P. C. and M. A. J. Rodgers (1983) Singlet molecular oxygen in micellar systems. 1. Distribution equilibria between hydrophobic and hydrophilic compartments. *J. Phys. Chem.* **87**, 4894–4898.
46. Lissi, E. A., E. Abuin, M. Saez, A. L. Zanocco and A. Disalvo (1992) Anomalous dependence of pyrene spectra and lifetimes with temperature in large unilamellar vesicles from dioctadecyldimethylammonium chloride and dipalmitoylphosphatidyl choline. *Langmuir* **8**, 348–350.
47. Lemp, E., A. L. Zanocco and G. Günther (2003) Structural changes in DODAC unilamellar liposomes by addition of sucrose esters monitored by using fluorescent techniques. *Colloids Surf. A Physicochem. Eng. Asp.* **229**, 63–73.
48. Lemp, E., A. L. Zanocco and E. A. Lissi (2003) Linear free energy relationship analysis of solvent effects on singlet oxygen reactions. *Curr. Org. Chem.* **7**, 799–819.
49. Carmona-Ribeiro, A. M. (1992) Synthetic amphiphile vesicles. *Chem. Soc. Rev.* **21**, 209–214.
50. Carmona-Ribeiro, A. M. and H. Chaimovich (1983) Preparation and characterization of large dioctadecyldimethylammonium chloride liposomes and comparison with small sonicated vesicles. *Biochim. Biophys. Acta* **733**, 172–179.
51. Martínez, L. A, C. G. Martínez, B. B. Klopoyek, J. Lang, A. Neuner, A. M. Braun and E. Oliveros (2000) Nonradiative and radiative deactivation of singlet molecular oxygen (O_2 ($a^1\Delta_g$)) in micellar media and microemulsions. *J. Photochem. Photobiol. B* **58**, 94–107.
52. Aubry, J.-M. and S. Bouttemy (1997) Preparative oxidation of organic compounds in microemulsions with singlet oxygen generated chemically by the sodium molybdate hydrogen peroxide system. *J. Am. Chem. Soc.* **119**, 5286–5294.